PAPER

Three-step self-calibrating generalized phase-shifting interferometry

To cite this article: Yu Zhang 2022 *Chinese Phys. B* **31** 030601

Three-step self-calibrating generalized phase-shifting interferometry

Yu Zhang(张宇)[1,2,†]

[1] *Institute of Materials Physics, College of Science, Northeast Electric Power University, Jilin* 132012, *China*
[2] *State Key Laboratory of Applied Optics, Changchun Institute of Optics, Fine Mechanics and Physics, Chinese Academy of Sciences, Changchun* 130022, *China*

(Received 7 July 2021; revised manuscript received 22 August 2021; accepted manuscript online 27 August 2021)

An accurate and fast three-step self-calibrating generalized phase-shifting interferomertry (SGPSI) is proposed. In this approach, two new phase-shifting signals are constructed by the difference interferograms normalization and noise suppressing, then the unknown phase shift between the two difference phase-shifting signals is estimated quickly through searching the minimum coefficient of variation of the modulation amplitude, a limited number of pixels are selected to participate in the search process to further save time, and finally the phase is reconstructed through the searched phase shift. Through the reconstruction of phase map by the simulation and experiment, and the comparison with several mature algorithms, the good performance of the proposed algorithm is proved, and it eliminates the limitation of requiring more than three phase-shifting interferograms for high-precision SGPSI. We expect this method to be widely used in the future.

Keywords: self-calibrating generalized phase-shifting interferomertry, phase shift, difference interferograms, modulation amplitude

PACS: 06.20.–f, 07.05.Kf, 07.60.Ly **DOI:** 10.1088/1674-1056/ac21c5

1. Introduction

Self-calibrating generalized phase-shifting interferometry (SGPSI) is a technique for extracting the phase map from three or more phase-shifting interferograms without knowing the phase shifts.[1] It removes the restriction that accurate phase-shifting interferometry (PSI) needs accurate phase shifter, thus, it has been widely used in high precision optical metrology. Over the past few decades, many ingenious SGPSIs have been developed, and they can be divided into iterative and non-iterative ones.[2]

Among the iterative SGPSIs, an overdetermined approach that uses least-squares algorithms has been studied extensively for randomly phase-shifting interferograms. In 2004, Wang proposed an advanced iterative algorithm (AIA), which can obtain accurate phase distribution from more than three randomly phase-shifting interferograms.[3] It resolves the limitation of the existing iterative phase-shifting algorithms (PSAs) and separates the frame-to-frame iteration from the pixel-to-pixel iteration. After that, many iterative PSAs based on AIA were proposed. In 2008, a new generalized iterative algorithm for extracting phase distribution from randomly and spatially nonuniform phase-shifting interferograms was proposed, it requires only four randomly phase-shifting interferograms, and finally an accurate phase map is extracted by reducing the effects of transition and tilt errors.[4] In 2019, Chen *et al.* evaluated the performance of AIA, and proposed an enhanced AIA (eAIA) which can control the phase shifts, frame numbers and suppress noise.[5] In general, the iterative SGPSI is relatively accurate, but the convergence of the algorithm requires more time. Moreover, a moderate number of interferograms are required to ensure high performance.

To save time, lots of non-iterative SGPSIs have been developed. In 2011, Vargas *et al.* designed a well-evaluated PSI based on the principal component analysis (PCA), which can obtain two orthogonal signals by PCA. It is very fast and requires very low computational requirements, so it can be used for very large images or very large image sets.[6] In 2015, Deng *et al.* presented an advanced principal component analysis method, two difference maps were obtained by a simple subtraction operation easily, and then the phase can be calculated by the traditional PCA.[7] From 2016 to 2017, Yatabe *et al.* proposed a series of PSAs based on PCA which can accurately extract the phase by integrating spatial information.[8–10] PCA is very fast, however, it needs to subtract the background intensity by acquiring more than three phase-shifting interferograms, and the phase shift should be well distributed between 0 and 2π. In addition, PCA needs to confirm the sign of the phase by extra method. In 2014, Wang *et al.* designed an advanced Gram–Schmidt orthonormalization algorithm (GS3), it needs only three phase-shifting interferograms. Although it costs less time than PCA, its accuracy is lower than PCA with more than three phase-shifting interferograms.[11] Non-iterative SGPSIs cost less time, however, their accuracies are lower than that of iterative SGPSIs.

Note that all these SGPSIs here can only deal with accuracy or computational time problem, and they are hard to get

†Corresponding author. E-mail: 20122412@neepu.edu.cn

high accuracy and high speed at the same time. In order to balance the speed and accuracy, it is essential to study the fast and accurate SGPSI.

In this paper, a fast and accurate three-step SGPSI to cope with the above problems is proposed. We first discuss the principles of the proposed method and then give its verification by computer simulations and experiments. Moreover, we compare the proposed method with AIA, PCA and GS3 to verify its outstanding performance.

2. Algorithm description

The expression of the i^{th} frame phase-shifting interferogram is

$$I_i(x,y) = a_i(x,y) + b_i(x,y)\cos\left(\varphi(x,y) + \theta_i\right), \tag{1}$$

where $a_i(x,y)$ and $b_i(x,y)$ respectively represent the background intensity and modulation amplitude of the interferograms, $\varphi(x,y)$ is the tested phase, θ_i is the phase shift, i represents the image index ($i = 1, 2, 3$), and the size of interferograms is $N_x \times N_y$. θ_1 can be considered to be zero without losing generality. The spatial coordinates have been omitted below for convenience.

Firstly, we implement the subtraction between the 1st phase-shifting interferogram and the i^{th} phase-shifting interferogram. Generally for the background intensity and modulation amplitude distributions, both the fluctuation between different interferograms and the non-uniformity between different pixels exist, however, the subtraction can still filter most of the background intensity. Hence, for simplicity, we assume that $a_i(x,y)$ and $b_i(x,y)$ are irrelevant to the image index, and only relevant to the pixel position in the subtraction process.

We calculate the intensity of difference maps between the 1st phase-shifting interferogram and the i^{th} phase-shifting interferogram as

$$D_1 = I_1 - I_2 = 2b\sin\left(\frac{\theta_2}{2}\right)\cos\left(\Phi'\right), \tag{2}$$

$$D_2 = I_1 - I_3 = 2b\sin\left(\frac{\theta_3}{2}\right)\cos\left(\Phi' + \Delta\right), \tag{3}$$

where $\Phi = \varphi + \frac{\theta_2}{2}$, $\Delta = \frac{\theta_3 - \theta_2}{2}$, and $\Phi' = \Phi - \frac{\pi}{2}$.

Then two difference vectors D_1 and D_2 were normalized by

$$\hat{D}_1 = \frac{D_1}{\|D_1\|} = \frac{b\cos\left(\Phi'\right)}{\sqrt{\sum_{N_x\times N_y} b^2\cos^2\left(\Phi'\right)}}, \tag{4}$$

$$\hat{D}_2 = \frac{D_2}{\|D_2\|} = \frac{b\cos\left(\Phi' + \Delta\right)}{\sqrt{\sum_{N_x\times N_y} b^2\cos^2\left(\Phi' + \Delta\right)}}, \tag{5}$$

where $\|\cdot\|$ represents the 2-norm.

When the number of fringes is more than one, there is an approximation as

$$\sqrt{\sum_{N_x\times N_y} b^2\cos^2\left(\Phi'\right)} \approx \sqrt{\sum_{N_x\times N_y} b^2\cos^2\left(\Phi' + \Delta\right)}. \tag{6}$$

Then, Eqs. (4) and (5) can be rewritten as

$$\hat{D}_1 = c\cos\left(\Phi'\right), \tag{7}$$

$$\hat{D}_2 = c\cos\left(\Phi' + \Delta\right), \tag{8}$$

where

$$c = \frac{b}{\sqrt{\sum_{N_x\times N_y} b^2\cos^2\left(\Phi'\right)}} = \frac{b}{\sqrt{\sum_{N_x\times N_y} b^2\cos^2\left(\Phi' + \Delta\right)}}.$$

Here $\hat{D}_1$ and $\hat{D}_2$ can be considered as two phase-shifting interference signals with no background intensity, Δ is the phase shift, and c represents the new modulation amplitude. The difference between φ and Φ' is a constant, which does not affect the phase distribution, so Φ' can express the tested phase. Because of the fluctuation, non-uniformity of the original modulation amplitude b and the approximation error of Eq. (6), the new modulation amplitude c is both relevant to the pixel position and image index. Hence Eqs. (7) and (8) are rewritten as

$$\hat{D}_m(x,y) = c_m(x,y)\cos\left(\Phi'(x,y) + \Delta_m\right), \tag{9}$$

where $m = 1, 2$ denotes the index of the new phase-shifting interference signals, $\Delta_1 = 0$ and $\Delta_2 = \Delta$.

To depress the noise, we use the mean of the adjacent pixels to generate the new pixel, then the new phase-shifting interferograms are generated. The distribution diagram of the adjacent pixels is shown in Fig. 1, and M is the number of adjacent pixels.

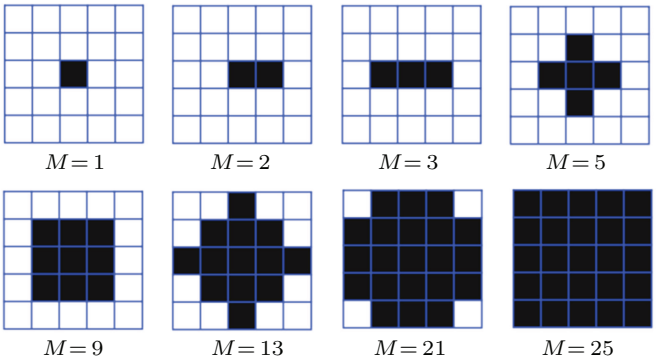

Fig. 1. Distribution diagram of the adjacent pixels.

Note that the boundary of new phase-shifting interference signals must be extended properly so that M adjacent pixels are valid, such as $\hat{D}_m(N_x + 1, N_y)$ is out of the range. According to the above eight situations in Fig. 1, we extend the size of the normalized difference maps from $N_x \times N_y$ to $(N_x + 4) \times (N_y + 4)$. The values of the 1st and the 2nd rows for the extended maps with the size of $(N_x + 4) \times (N_y + 4)$ are

the same as that of the 1st row for the original maps with the size of $N_x \times N_y$. The values of the $(N_x+3)^{\text{th}}$ and the $(N_x+4)^{\text{th}}$ rows for the extended maps are the same as that of the N_x^{th} row for the original maps. Moreover, the values of the 3rd to the $(N_x+2)^{\text{th}}$ rows for the extended maps are the same as that of the 1st to the $(N_x)^{\text{th}}$ rows for the original maps. Finally, the extension of the column is the same as the row.

The expression of the new phase-shifting interferograms can be written as

$$W_m = \eta \cos\left(\Phi' + \delta_m\right), \tag{10}$$

where η and δ_m represent the modulation amplitude and phase shift, respectively, and we set δ_1=0 and $\delta_2 = \delta$.

According Eq. (10), η can be expressed as a function of δ

$$\eta = \sqrt{W_1^2 + \left[\frac{W_1}{\tan(\delta)} - \frac{W_2}{\sin(\delta)}\right]^2}. \tag{11}$$

The coefficient of variation (CV) of η is defined as

$$\mathrm{CV}(\eta) = \frac{\mathrm{std}(\eta)}{\mathrm{mean}(\eta)}, \tag{12}$$

where $\mathrm{std}(\cdot)$ denotes the standard deviation, and $\mathrm{mean}(\cdot)$ denotes the mean value. The normalization to the mean can make this quantity independent of different measurements. According to Eq. (12), CV can be used as a parameter to evaluate the variation of the modulation amplitude η. η will be irrelevant to the pixel position and image index ideally. However, because of the fluctuation, non-uniformity of the original modulation amplitude b, the approximation error of Eq. (6) and noise depression error, η is both relevant to the pixel position and image index. Although η is not a constant for different pixel positions, the difference between different pixels will also be very small. Hence, when the phase shift δ is accurate, η is also accurate, and CV will be minimum, so the phase shift δ can be determined through searching the minimum of CV,

$$\delta = \arg\min_{\delta} \mathrm{CV}(\eta). \tag{13}$$

Finally, the phase can be obtained by

$$\Phi' = \tan^{-1}\frac{W_1\cos(\delta) - W_2}{W_1\sin(\delta)}. \tag{14}$$

In order to further save time, a limited of pixels with equal interval can be chosen to take part in the searching process.

3. Simulation verification

The validity of the proposed method have been verified by the numerical simulations. In the following, all computations are performed with the CPU of Intel(R) Core(TM) i5-8265U and the 8 GB memory, and we use the Matlab software for coding.

Firstly, we simulate the circular fringes, the background intensity and modulation amplitude are set as $a_i(x,y) = N_a \exp\left[-0.02\left(x^2+y^2\right)\right]$ and $b_i(x,y) = N_b \exp\left[-0.02\left(x^2+y^2\right)\right]$, respectively, with $-1 \le x \le 1$ and $-1 \le y \le 1$. Generally, the background intensity and modulation amplitude have frame-to-frame fluctuation, hence, N_a of the 1st, 2nd and 3rd interferograms are set as 1, 0.95 and 0.9, N_b of the 1st, 2nd and 3rd interferograms are set as 0.9, 0.85 and 0.8, the phase is set as $\varphi(x,y) = 4\pi\left(x^2+y^2\right)$, the phase shifts are 0, 1 and 3 rad, and the noise satisfies the Gaussian distribution, whose signal-to-noise ratio (SNR) is 20 dB. The background intensity, modulation amplitude and theoretical phase maps and three phase-shifting interferograms are shown in Figs. 2(a)–2(f). The normalized difference signals without the background intensity as Eqs. (7) and (8) are given by Figs. 2(g) and 2(h). To choose the optimal M and number of chosen pixels searching the minimum of CV, we test the proposed method with different M and number of chosen pixels. Figures 2(i) and 2(j) present the root mean square (RMS) phase errors and computational time of the proposed method with different M, and it can be seen that, when M is increasing, the RMS phase error is decreasing, and large M costs only a little more time than small M. Figures 2(k) and 2(l) show the RMS phase errors and computational time of the proposed method when the number of chosen pixels is different, and we can see that the RMS phase errors are similar for different number of chosen pixels, especially when the number of chosen pixels is larger than 41×41, and the RMS phase errors are the same. When the number of chosen pixels is less than 101×101, it costs relatively less time, otherwise, it takes more time to compute. In summary, when the noise of the phase-shifting interferograms with 401×401 pixels is 20 dB, the optimal number of chosen samples is 41×41, the optimal M is 25, and it can obtain high accuracy and high speed at the same time.

Figures 2(m) and 2(n) present the new phase-shifting interferograms after suppressing the noise as Fig. 1 ($M = 25$), and we can see that the new phase-shifting interferograms are more clear than the original phase-shifting interferograms. After calculating the CV of the modulation amplitude with different phase shifts (the number of chosen samples is 41×41), Fig. 2(o) is obtained, and the phase shift between Figs. 2(m) and 2(n) corresponding to the valley can be just used to rebuild the phase map. The rebuilt phase map using the found phase shift and phase error map are given in Fig. 2(p) (note that, there are two steps to obtain the phase error map, firstly, we implement the subtraction between the rebuilt phase map and theoretical phase map, then we subtract the minimum from the existing phase error map), and the results of AIA method and

PCA/GS3 method are shown in Figs. 2(q) and 2(r). We calculate the RMS of phase error and computational time, as listed in Table 1. From Figs. 2(p)–2(r) and Table 1, it can be seen that the accuracy of the proposed method is higher than that of AIA, PCA and GS3, and it costs relatively less time, the accuracy of PCA and GS3 are same, but GS3 costs less time.

We also study the effect of noise to the optimal M, and the number of chosen pixels is 41×41. Figure 2(s) shows the results, and it can be seen that, if the SNR is 20 dB, when M is increasing, the phase error is decreasing, and for other situations, when M is equal to 2, the phase error is maximum due to the asymmetric error of the adjacent pixels (see Fig. 1). In fact, for any level of noise, the asymmetric error always exists when M is equal to 2, however, the effect of 20 dB of noise is larger than that of the asymmetric error. In the actual experiments, the level of noise is unknown, so it is best not to set M equal to 2 to avoid the effect of asymmetric error. In addition, if the SNR is greater than 30 dB, the phase error when M is equal to 3 is minimum. Therefore, it can be concluded that the optimal M is 25 when the SNR is 20 dB, and the optimal M is 3 if the SNR is greater than 30 dB. Although the optimal M is different for different levels of noise, when M is equal to 3, the phase error with 20 dB noise is also relatively small, therefore, 3 can be chosen as the common M in different cases.

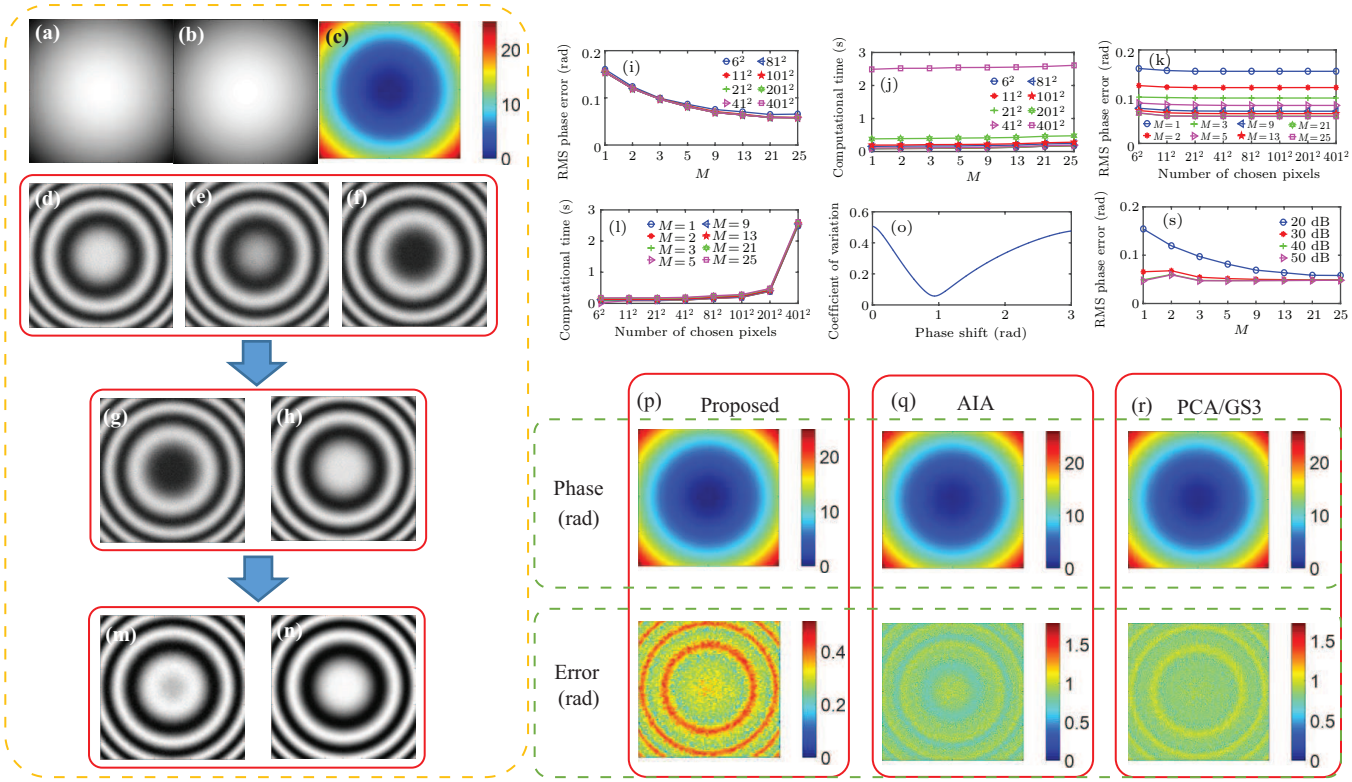

Fig. 2. Illustration of the proposed method with simulated circular fringes. (a) and (b) Background intensity and modulation amplitude maps. (c) Theoretical phase map. (d)–(f) Three simulated interferograms (size: 401×401) with phase shifts $\theta = (0, 1, 3)$ rad. (g) and (h) Normalized difference signals as Eqs. (7) and (8). (i) and (j) RMS phase errors and computational time with different M. (k) and (l) RMS phase errors and computational time with different number of chosen pixels. (m) and (n) New phase-shifting interference signals of Eq. (10). (o) Coefficients of variation calculated by Eq. (12). (p)–(r) Reconstructed phase maps and phase error maps from the proposed, AIA, and PCA/GS3 methods, respectively. (s) RMS phase errors with different M for different levels of noise.

It is interesting to analyze the performance of the proposed method, AIA, PCA and GS3 with various phase shifts. For the proposed method, M is chosen as 25, the number of chosen pixels is 41×41, and other conditions remain unchanged as the circular fringes. The phase shifts of the 1st and 2nd phase-shifting interference signals remain the same, and the phase shift of the 3rd phase-shifting signal is changed from 1.3 rad to 6.0 rad. Figure 3(a) shows the results, and it can be seen that the phase error varies with the change of the phase shift with regard to different methods, and the closer to 1.3 rad and 6 rad, the larger the RMS phase error is, when the practical phase shift $(\theta_3 - \theta_2)/2$ is close to 0 rad or π rad, and the RMS phase error will be significantly large. In addition, the range of phase shift of the proposed method is larger than that of other methods. In the whole range of phase shift, the accuracy of the proposed method is higher than that of other methods, and the accuracies of AIA and PCA/GS3 are similar for most of the phase shifts. Moreover, we also simulate the situation of small phase shifts, such as the phase shifts are set as 0, 0.1 rad and 0.2 rad. When the SNR of noise is greater than 50 dB, all methods work, otherwise, they do not work because of the large noise. In the actual experiment, the noise distribution is more complex and must exist, so very small phase shifts are not suitable for general methods, including the proposed

method. In the future work, we may find or study a method to slove this problem.[12]

We also test the proposed method at different levels of noise in Fig. 3(b), compared with the current well-evaluated SGPSI. The accuracy of the proposed method is higher than that of AIA, PCA/GS3, and they are almost stable for different levels of noise. If the SNR of noise is less than 40 dB, the RMS phase error of AIA, PCA/GS3 is decreasing with the decrease of the noise, and if the SNR of noise is greater than 40 dB, they are all stable. Moreover, the RMS phase error of PCA/GS3 is large as AIA when the noise is large, but it can be similar to the proposed method if the SNR of noise is greater than 40 dB. From the above analysis, we can conclude that the proposed method is more insensitive to the noise, and suitable for any levels of noise.

As mentioned before Eq. (6), the proposed method requires more than one fringe in the interferograms. In fact, if the number of fringes is less than one, the phase error may be relatively large, but it can also reconstruct the phase distribution. To verify this point, we compute the RMS phase errors with different number of fringes from 0 to 4, and the other parameters are same as Figs. 2(d)–2(f). Figure 3(c) presents the results, the RMS phase errors of all methods are almost invariable if the number of fringes is larger than one. However, when there is less than one fringe in the interferograms, the performance of AIA, PCA/GS3 gets worse. By contrast, the proposed method always performs well.

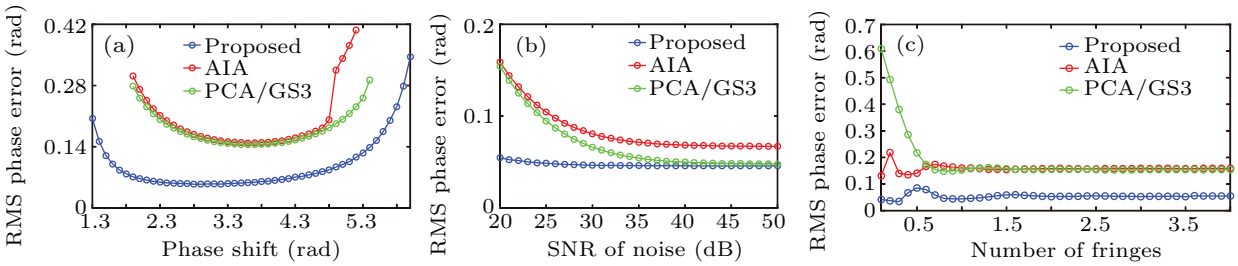

Fig. 3. Comparisons on the RMS phase errors between different methods. (a) RMS phase errors with different phase shifts θ_3 ($\theta_1 = 0$, $\theta_2 = 1$ rad). (b) RMS phase errors with different levels of noise. (c) RMS phase errors with different number of fringes.

We also simulate the complex fringes, the phase is set as $\varphi(x,y) = 4x^2 + 4y^2 + 4x^3 + 4y^3 + 4\text{peaks}(401)$, other conditions are the same as the circular fringes, and finally the conclusion is the same as the circular fringes. As shown in Fig. 4 and Table 1,we can conclude that the proposed method is accurate and efficient for different kinds of fringes.

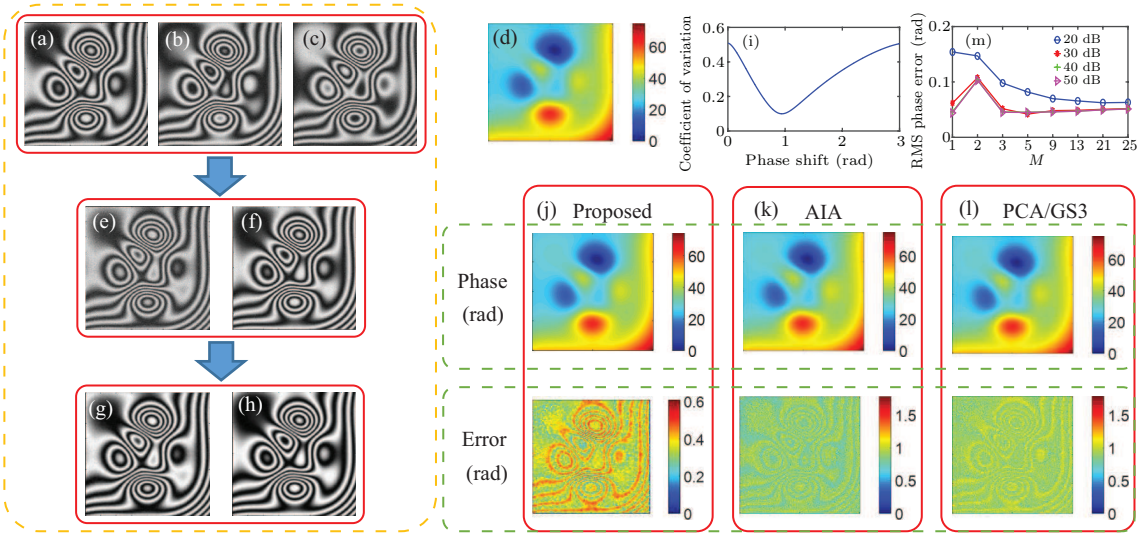

Fig. 4. Illustration of the proposed method with simulated complex fringes. (a)–(c) Three simulated interferograms (size: 401×401) with phase shifts $\theta = (0,1,3)$ rad. (d) Theoretical phase map. (e) and (f) Normalized difference signals as Eqs. (7) and (8). (g) and (h) New phase-shifting interference signals of Eq. (10). (i) Coefficients of variation calculated by Eq. (12). (j)–(l) Reconstructed phase maps and phase error maps from the proposed, AIA, and PCA/GS3 methods, respectively. (m) RMS phase errors with different M for different levels of noise.

4. Demonstration with experimental data

The performance of the proposed method is also verified by the experimental interferograms with different kinds of fringes. Four phase-shifted interferograms with the phase shifts 0, $\pi/2$, π, and $3\pi/2$ are acquired by the snapshot phase-shifting interferometer, the phase shift error will be very small because only a single image snapshotted is extracted by the polarization camera, and the highly accurate phase extracted by standard 4-step PSI can be set as the reference phase. Ac-

cording to the conclusion of above simulations, the number of chosen pixels to search the minimum CV with different phase shifts is set as 41×41. The interferograms with circular fringes are shown in Figs. 5(a)–5(d), and the reference phase map is shown in Fig. 5(e). The normalized difference signals without the background intensity are presented in Figs. 5(f)–5(g), the curve of RMS phase errors with various M is plotted in Fig. 5(h), and it can be seen that, when M is equal to 3, the RMS phase error is minimum, and it is the same as the simulation with the SNR of noise greater than 30 dB. Therefore, 3 can be chosen as the optimal M. The new phase-shifting interferograms after suppressing the noise are presented in Figs. 5(i) and 5(j), after calculating the CV of the modulation amplitude with different phase shifts (Fig. 5(j)), the phase shift between the new phase-shifting interferograms corresponding to the valley can be just used to reconstruct the phase map, the difference map between the reference and rebuilt phase maps is regarded as the phase error map, and then subtract the minimum from the existing phase error map, the phase and phase error maps are shown in Fig. 5(l), and the results of AIA, PCA/GS3 are given in Figs. 5(m) and 5(n).

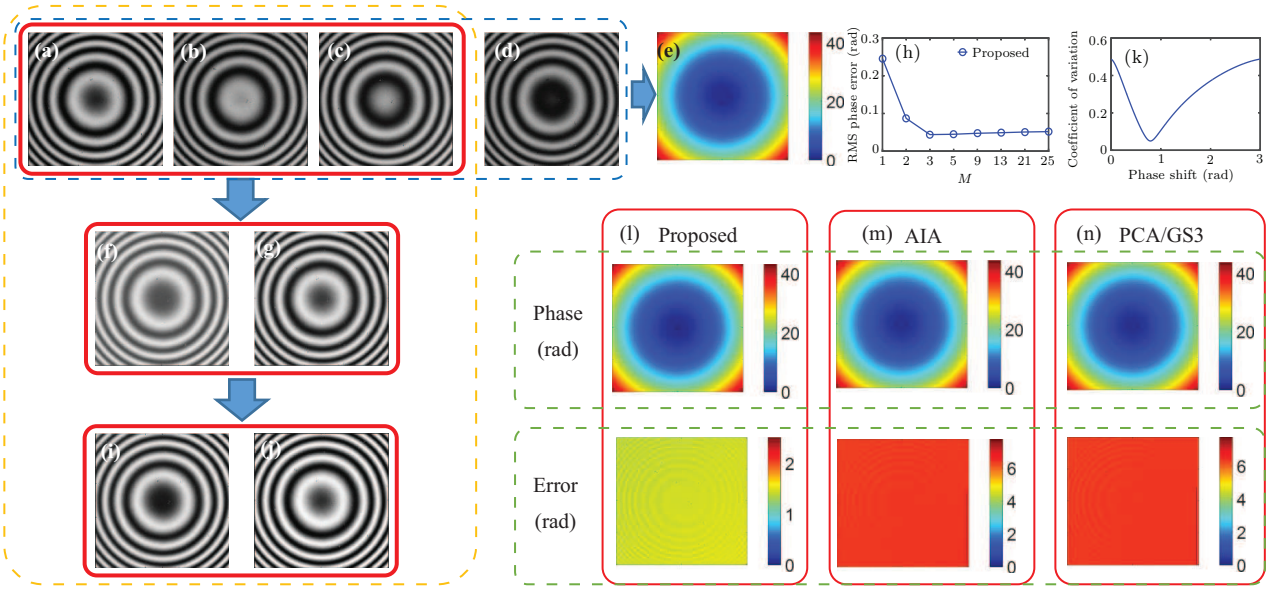

Fig. 5. Experimental phase reconstruction with circular fringes. (a)–(d) Four interferograms (size: 401×401) with phase shifts $\theta = (0, \pi/2, \pi, 3\pi/2)$ rad. (e) Reference phase map calculated by standard 4-step PSI. (f) and (g) Normalized difference signals as Eqs. (7) and (8). (h) RMS phase errors with different M. (i) and (j) New phase-shifting interference signals of Eq. (10). (k) Coefficients of variation calculated by Eq. (12). (l)–(n) Reconstructed phase maps and phase error maps from the proposed, AIA, and PCA/GS3 methods.

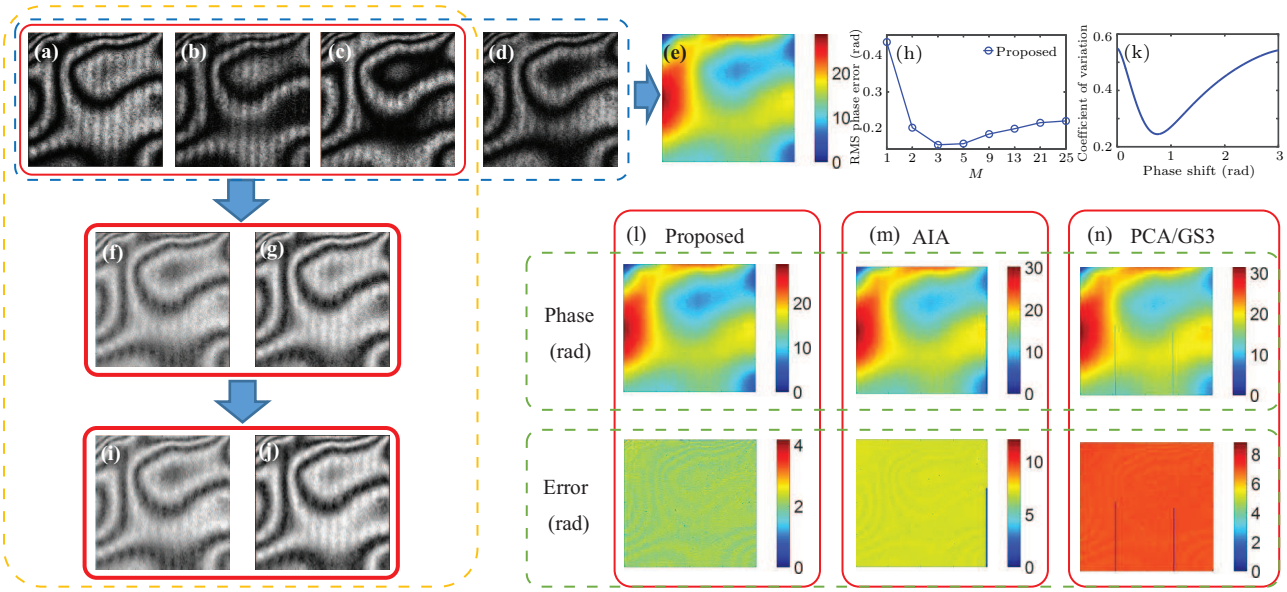

Fig. 6. Experimental phase reconstruction with complex fringes. (a)–(d) Four interferograms (size: 201×201) with phase shifts $\theta = (0, \pi/2, \pi, 3\pi/2)$ rad. (e) Reference phase map calculated by standard 4-step PSI. (f) and (g) Normalized difference signals as Eqs. (7) and (8). (h) RMS phase errors with different M. (i) and (j) New phase-shifting interference signals of Eq. (10). (k) Coefficients of variation calculated by Eq. (12). (l)–(n) Reconstructed phase maps and phase error maps from the proposed , AIA, and PCA/GS3 methods.

We also test the proposed method, AIA, PCA and GS3 with experimental complex fringes from a deformable mirror, as shown in Fig. 6, where the optimal M is also 3. The RMS of phase errors and computational time of different methods are listed in Table 1. From Figs. 5, 6 and Table 1, if $M = 1$, the RMS phase error is so large because the phase map after unwrapping is unsmooth, so the suppression of noise is very important, and the RMS phase errors of AIA, PCA and GS3 are also large due to the same reason as the proposed method with the situation of $M = 1$. For the experiment, whether the background intensity and modulation amplitude distributions or the noise distribution may be more complex than the simulation, and PCA and AIA generally need more than three interferograms to obtain good performance, hence when the conditions are more complex, they do not work. However, the proposed method is suitable for different experimental conditions, and it can obtain highly accurate phase map and cost relatively less time simultaneously with only three randomly phase-shifting interferograms.

Table 1. RMS phase errors and computational time via proposed, AIA, PCA and GS3 methods.

		Proposed	AIA	PCA	GS3
Fig. 2	RMS phase error (rad)	0.058	0.159	0.155	0.155
	Time (s)	0.190	17.123	0.094	0.005
Fig. 4	RMS phase error (rad)	0.063	0.160	0.155	0.155
	Time (s)	0.191	16.641	0.095	0.005
Fig. 5	RMS phase error (rad)	0.044	0.246	0.246	0.246
	Time (s)	0.187	18.216	0.012	0.006
Fig. 6	RMS phase error (rad)	0.207	0.389	0.430	0.430
	Time (s)	0.095	5.599	0.006	0.003

5. Conclusions

In conclusion, an accurate and timesaving three-step self-calibrating phase-shifting interferometry is proposed. Both simulated and experimental results indicate that the proposed method can reconstruct the accurate phase map with high efficiency, even compared with the well-evaluated SGPSIs-AIA, PCA and GS3. Moreover, the proposed method performs well in different phase shifts, levels of noise and number of fringes. Lastly, the proposed method is suitable for different kinds of fringes and experimental conditions. We expect this method to be widely used in the future.

Acknowledgements

Project supported by the National Natural Science Foundation of China (Grant No. 61905039), Jilin Scientific and Technological Development Program, China (Grant No. 20190701018GH), Education Department of Jilin Province, China (Grant No. JJKH20190691KJ), and State Key Laboratory of Applied Optics.

References

[1] Meneses-Fabian C and Tejeda-Muñoz N 2017 *Appl. Opt.* **56** 4278
[2] Malacara D 2007 *Optical Shop Testing*, 3rd edn (New Jersey: John Wiley & Sons) pp. 568–591
[3] Wang Z 2004 *Opt. Lett.* **29** 1671
[4] Xu J, Xu Q and Chai L 2008 *Appl. Opt.* **47** 480
[5] Chen Y, Lin P, Lee C and Liang C 2013 *Appl. Opt.* **52** 3381
[6] Vargas J, Quiroga J and Belenguer T 2011 *Opt. Lett.* **36** 1326
[7] Deng J, Wang K, Wu D, Lv X, Li C, Hao J, Qin J and Chen W 2015 *Opt. Express* **23** 12222
[8] Yatabe K, Ishikawa K and Oikawa Y 2016 *Opt. Express* **24** 22881
[9] Yatabe K, Ishikawa K and Oikawa Y 2017 *J. Opt. Soc. Am. A* **34** 87
[10] Yatabe K, Ishikawa K and Oikawa Y 2017 *Opt. Express* **25** 29401
[11] Wang H, Luo C, Zhong L, Ma S and Lu X 2014 *Opt. Express* **22** 5147
[12] Deng J, Wu D, Wang K and Vargas J 2016 *Sci. Rep.* **6** 24416